Jetting and Droplet Formation Driven by Interfacial Electrohydrodynamic Effects Mediated by Solitons in Liquid Crystals

Soumik Das,[1] Noe Atzin,[2] Xingzhou Tang,[2] Ali Mozaffari,[2] Juan de Pablo,[2] and Nicholas L. Abbott[1,*]

[1]*Smith School of Chemical and Biomolecular Engineering, Cornell University, Ithaca, New York 14853, USA*
[2]*Pritzker School of Molecular Engineering, University of Chicago, Chicago, Illinois 60637, USA*

Solitons are highly confined, propagating waves that arise from nonlinear feedback in natural (e.g., shallow and confined waters) and engineered systems (e.g., optical wave propagation in fibers). Solitons have recently been observed in thin films of liquid crystals (LCs) in the presence of ac electric fields, where localized LC director distortions arise and propagate due to flexoelectric polarization. Here we report that collisions between LC solitons and interfaces to isotropic fluids can generate a range of interfacial hydrodynamic phenomena. We find that single solitons can either generate single droplets or, alternatively, form jets of LC that subsequently break up into organized assemblies of droplets. We show that the influence of key parameters, such as electric field strength, LC film thickness, and LC-oil interfacial tension, map onto a universal state diagram that characterizes the transduction of soliton flexoelectric energy into droplet interfacial energy. Overall, we reveal that solitons in LCs can be used to focus the energy of nonlocalized electric fields to generate a new class of nonlinear electrohydrodynamic effects at fluid interfaces, including jetting and emulsification.

Nonequilibrium states of soft matter that form via the dissipation of energy are the basis of biological processes central to life (e.g., cell division) [1]. Such states of matter often arise from highly nonlinear phenomena that generate strongly localized responses to delocalized stimuli [1–4]. Solitons in liquid crystals (LCs) represent one such class of nonlinear phenomena with the potential to provide fundamental insights into the transfer of energy, chemical species, and information that accompanies solitons in biological and synthetic soft matter [5–12]. Solitons in LC films are observed as highly localized and rapidly propagating LC director fluctuations that are triggered by external fields [8,9,13–17,20–23]. Several mechanisms have been proposed to lead to the formation of LC solitons in ac electric fields, including flexoelectric, dielectric, and electrohydrodynamic effects [8,9,11–14] (see section S1 in [15]). Recent computational studies reveal that propagating bulletlike solitons can form in the absence of ions when a surface chemical or topographical feature generates a quadrupolar distortion of the LC following application of a weak ac field [24,25]. At higher electric field strengths, the symmetry of the quadrupolar state is broken by the flexoelectric energy, driving the formation of a propagating soliton [Figs. 1(a) and 1(b)]. The largest contribution to the soliton energy was shown to arise from flexoelectric polarization, indicating that solitons can be viewed as propagating packets of flexoelectric energy.

The interactions of electric fields and fluids generate a rich range of electrohydrodynamic (EHD) phenomena [26] at fluid-fluid interfaces, including electrojetting [27], equatorial streaming [28], emulsion breakup, and coalescence [29–32]. EHD flows often arise from unbalanced Maxwell's stresses acting at fluid interfaces, where the stress is generated by an accumulation of charge density due to distinct permittivities and/or ionic conductivities of two fluids [26,33]. In contrast to these past reports, our results reveal that flexoelectric effects in LCs can generate solitons that, upon collision with the interface to an isotropic liquid, lead to localized charging and a new class of EHD interfacial phenomena.

Initially, we performed experiments using squalane and 4′-butyl-4-heptyl-bicyclohexyl-4-carbonitrile (CCN-47, Table S1 in Supplemental Material [15]) because they form a biphasic system with a low interfacial tension (0.02 mN/m) (see sections S2 and S3 for discussion on experimental methodologies [15]). In addition, we found the interface between the squalane-rich and CCN-47-rich phases to be stable at voltages lower than those that generated solitons, and also to not exhibit any measurable perturbation when solitons were present in the LC domains far from the interface between the squalane-rich phase and LC [see Fig. 1(c)].

Next, we examined the response of the LC-squalane interface to a collision with a single soliton propagating from the LC [Figs. 1(c)–1(f)]. In the example shown in Fig. 1(c), the soliton was generated by applying 50 V at 517 Hz across a LC film with thickness of 8 μm. The angle between the normal to the squalane–CCN-47 interface and the LC director was 55°; optical characterization under crossed polars (Fig. S5 in Supplemental Material [15])
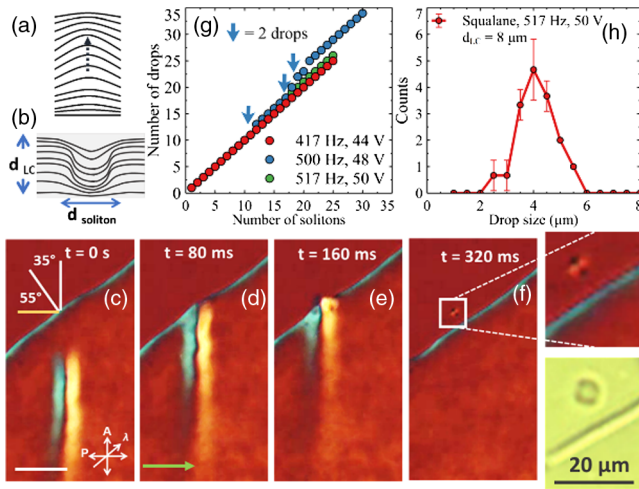
FIG. 1. (a),(b) Schematic illustration depicting the (a) azimuthal and (b) polar LC director orientations within a soliton propagating along the direction of the dotted arrow (c)–(f) Timed snapshots (crossed polars and a red plate compensator inserted at 45° from the polars) showing formation of a LC droplet following collision of a soliton with the LC-isotropic oil interface. Insets in (f) show bright-field and cross-polar images of the LC droplet. The applied voltage is 517 Hz, 50 V. Green arrows indicate the direction of gold deposition. Scale bar 30 μm. (g) Number of generated LC drops as a function of number of solitons hitting the interface at different applied electric fields. (h) Size distribution of generated LC drops.

FIG. 2. (a)–(f) Bright-field images showing the nematic CCN-47–squalane interface following the collision of a single soliton with the interface. The brown arrows in (a) and (b) indicate the incident soliton traveling at an angle 45° with respect to the interface. The dashed line in (a) indicates the CCN-47–squalane interface. The dashed line in (b) and (c) indicates the centerline of the soliton. The left wing of the soliton collides first with the interface and forms a jet indicated by the brown curved arrow in (c). The droplet generated by the soliton collision is indicated by arrows in (e) and (f). Scale bar 15 μm. The black arrows in (c) and (d) point to LC director perturbations in the LC that are generated by the right wing of the soliton. (g),(h) Cross-polar images showing the director perturbations in the LC near the interface after a collision with a soliton. The white arrows in (g) and (h) indicate the propagating soliton and the LC jet, respectively. The yellow arrow in (h) shows the director perturbations created by the right wing of the soliton. Scale bar 15 μm. Image contrast in (a)–(h) has been enhanced for visualization. (i) Sizes of LC drop generated for two different LC film thicknesses. The red and blue bars correspond to 8-μm- and 12-μm-thick LC films.

confirmed the presence of strain in the LC near the interface because the LC anchors parallel to the interface of the isotropic domain (planar anchoring). Because the soliton propagates in a direction perpendicular to the LC director in the bulk LC, the angle between the incident soliton and the interface normal was 35°. We measured the width of the soliton to be 8 μm (see Fig. S6 for definition of soliton width [15]) and the velocity to be 440 μm/s. Inspection of Figs. 1(d) and 1(e) reveals that the interface between the LC and isotropic oil was transiently deformed upon impact by the soliton, with the interface and the LC director within the LC continuous domain returning within 300 ms to a state indistinguishable from that observed prior to impact of the soliton [Fig. 1(f)]. Further inspection of Fig. 1(f), however, reveals the presence of a single LC microdroplet (confirmed by cross-polar micrographs; see inset of Fig. 1(f) herein and Fig. S7 in Ref. [15]) with a diameter of approximately 4.2 μm located in a region of the isotropic oil that was 8 μm from the location of impact of the soliton. Additional observations confirmed that, under conditions similar to the experiment shown in Fig. 1 (i.e., angles between incident soliton and interface normal of 30°–70°), most soliton collisions with the interface resulted in the generation of a single LC microdroplet in the oil phase [Fig. 1(g)]. We characterized the size distribution of the LC droplets [Fig. 1(h)] and determined the average size to be 3.8 ± 0.6 μm. We also observed that a small fraction of

solitons (1%–3%) formed multiple drops from a single collision event [≤3 drops; see data points corresponding to 517 Hz, 48 V in Fig. 1(g) herein and Fig. S8 in Ref. [15]]. We observed LC microdroplets to form from the collisions of solitons when using a range of applied voltages and frequencies [Fig. 1(g)]. Furthermore, when multiple solitons collided sequentially at the same location on the LC interface, we observed the number of LC emulsion droplets formed to be equal to the number of solitons (Fig. S9 [15]), revealing a high level of control over droplet generation using solitons. We refer to this process as solitonic emulsification.

To provide insight into the pathway that underlies solitonic emulsification, we obtained sequential bright-field images of the LC-oil interface during a soliton collision (generated by applying an ac field of 517 Hz, 48 V) [Figs. 2(a)–2(f)]. We make three key observations from Fig. 2. First, within 80 ms of the soliton collision, a small jet of LC [Fig. 2(c); with diameter ~3 μm] is observed to extend a distance of 12–14 μm into the isotropic oil from the soliton impact location. Subsequently, the LC jet forms a neck [Fig. 2(d)] that pinches off into a single LC droplet

[Fig. 2(f)]. Second, close inspection of Figs. 2(a)–2(c) reveals that the LC jet does not form at the centerline of the soliton [see Fig. 2(b); the centerline of the soliton is indicated by a dashed line] but instead forms at the location of the left "wing" of the soliton. Specifically, the side of the soliton that collides first with the interface [left half of soliton in Fig. 2(b)] defines the location at which the LC jet is generated (Fig. S11 in Ref. [15]). In contrast, the right wing of the soliton causes only a small displacement of the interface [Fig. 2(c)], which is rapidly damped [Figs. 2(d)–2(f)]. However, under crossed polar imaging, it is apparent that the right half of the soliton generates a director perturbation that traverses a distance of ∼14 μm along the interface of the continuous LC domain [Fig. 2(c)]. Additional experiments confirmed these observations [Figs. 2(g) and 2(h) herein and Fig. S12 in Ref. [15]]. Third, while the direction along which the LC jet extended from the interface was initially collinear with the trajectory of the incident soliton, Fig. 2(c) reveals that the LC jet bends toward the interface of the continuous LC domain as the director perturbations associated with the right half of the soliton propagates along the LC interface [Fig. 2(d)]. This result hints at the presence of a hydrodynamic coupling between the LC jet and the director perturbation that propagates along the interface, a point that we return to below.

The results shown in Figs. 2(a)–2(f) are qualitatively consistent with a process in which the transformation of the LC jet into an isolated LC drop is driven by capillary forces [34–37]. We determined that fluid inertia is small compared to viscous forces and that capillary forces are comparable to viscous forces (see section S4 in Supplemental Material [15]) [36–38]. The latter force balance predicts the droplet size to scale as

$$d \sim \gamma_{\text{LC-oil}} d_{\text{jet}} / \mu_{\text{oil}} V, \qquad (1)$$

where d_{jet} is the diameter of the LC jet. Equation (1) predicts that a soliton propagating at $V \sim 450 \ \mu\text{m s}^{-1}$ will generate a droplet size of $d \sim 4.5 \ \mu\text{m}$ from a 3-μm-diameter LC jet (Fig. S13 [15]) formed at the CCN-47–squalane interface, a prediction that is in good agreement with our experimentally observed drop sizes of $3.8 \pm 0.6 \ \mu\text{m}$. By noting that d_{jet} varies linearly with d_{soliton} and $d_{\text{soliton}} \approx d_{\text{LC}}$ (Figs. S13 and S14 in Ref. [15]), where d_{soliton} is the half-width of the soliton, we conclude that the soliton size and thickness of the LC film control the LC droplet size [Fig. 2(i) herein and Fig. S15 [15]].

To test the proposal that LC droplet formation is regulated by the transduction of flexoelectric energy into interfacial energy, we estimated the flexoelectric energy of a propagating soliton as

$$E_{\text{flexo}} \sim e U d_{\text{soliton}}, \qquad (2)$$

where e is the effective flexoelectric coefficient for CCN-47 ($e \sim 10^{-11} \ \text{C m}^{-1}$) and U is the applied voltage [8].
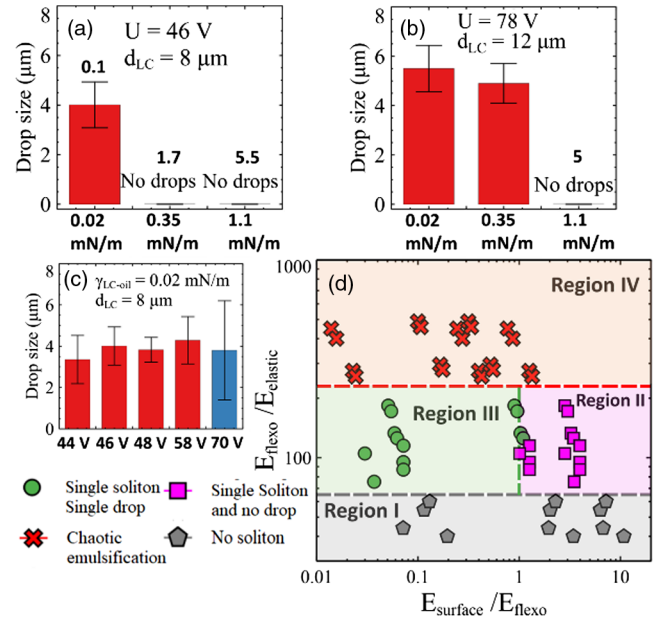
FIG. 3. (a),(b) LC droplet sizes generated by solitons as a function of $\gamma_{\text{LC-oil}}$ and two values of d_{LC}: (a) 8 μm and (b) 12 μm. The numbers above the bars indicate the ratio of E_{surface} to E_{flexo}. (c) LC droplet sizes generated by solitons, as a function of applied voltage. The blue bar corresponds to the chaotic emulsification regime. (d) State diagram showing the final state of the interface as a function of the relative magnitudes of normalized interfacial and flexoelectric energies.

The interfacial energy was evaluated as

$$E_{\text{surface}} = \pi d^2 \gamma_{\text{LC-oil}} / 4. \qquad (3)$$

Equations (2) and (3) predict that the relative magnitudes of the flexoelectric and interfacial energies can be independently manipulated by varying $\gamma_{\text{LC-oil}}$, U, and d_{soliton}. For the case of 8-μm-thick films of CCN-47 and squalane, and conditions under which solitons generated LC microdroplets [Fig. 3(a)], we found the ratio of E_{surface} to E_{flexo} to be around 0.1 (Fig. S16 in Supplemental Material [15]). In contrast, when using 8-μm-thick films of CCN-47 and castor oil, we did not observe LC microdroplets to be generated by solitons [Fig. 3(a); no drop formation for $\gamma_{\text{LC-oil}} = 0.35$ mN/m]. For castor oil, $\gamma_{\text{LC-oil}}$ is higher than squalane, and we calculate E_{surface} to be larger than E_{flexo} for droplets of size ∼4 μm (half-width of soliton size). We considered the possibility that LC drops of smaller sizes, with smaller interfacial energies, might be generated by castor oil. However, we did not observe formation of microdrops smaller than 4 μm in our experiments, providing further support for our previous conclusion that the sizes of the microdroplets generated during solitonic emulsification are set by the sizes of the solitons and LC film thickness [Fig. 2(i)].

Guided by Eq. (2), we predicted that the energy content of a propagating soliton can be increased by increasing the

LC film thickness because both U and $d_{soliton}$ increase with the LC film thickness (under conditions where single solitons form). Our experimental observations supported this prediction. Specifically, we found that, upon increasing the LC film thickness to 12 μm, propagating solitons were able to trigger LC droplet formation at the CCN-47/castor oil interface [Fig. 3(b) herein and Fig. S17 in Ref. [15]]. We estimated the flexoelectric and interfacial energies for this combination of components and LC film thickness, and found that E_{flexo} is close to or greater than $E_{surface}$ (Fig. S16 [15]). We also increased U at fixed $\gamma_{LC\text{-}oil}$ and LC film thickness, and we observed a gradual evolution in behavior, from a regime of focused droplet formation to a chaotic behavior at high voltages that was characterized by a broad drop size distribution [Fig. 3(c); see below for additional discussion]. To further confirm the role played by the relative magnitudes of $E_{surface}$ and E_{flexo} during solitonic emulsification, we used phenylmethylsiloxane-dimethylsiloxane copolymer as an isotropic oil that generates a high $\gamma_{LC\text{-}oil}$ (1.1 mN/m). When using this oil, no LC drops were generated when using either 8-μm- or 12-μm-thick LC films [Figs. 3(a) and 3(b) herein and Fig. S18 [15]].

We found that the various observations described above could be mapped onto a state diagram that quantifies the normalized flexoelectric and interfacial energies [Fig. 3(d)]. The flexoelectric energy normalized by the elastic energy ($E_{elastic} \sim Kd_{LC}$; K is the elastic constant) characterizes the ability of the applied electric field to generate solitons. The interfacial energies normalized by the flexoelectric energy indicate the availability of flexoelectric energy in a soliton for transduction into LC droplet interfacial energy (equal magnitudes indicated by the dotted green line). The state diagram contains four distinct regions. When the applied electric field is low, the flexoelectric energy is unable to overcome the elastic energy and we do not observe the formation of solitons [region I in Fig. 3(d)]. In region II, the applied electric field is sufficient to generate solitons, but the interfacial energy needed to form LC drop exceeds the flexoelectric energy and thus solitons are seen without the formation of LC droplets [region II in Fig. 3(d)]. In region III, flexoelectric energy is sufficient to form solitons and provide the interfacial energy of a single LC drop. Region V corresponds to high flexoelectric energies, achieved by increasing the applied voltage. Under these conditions, the solitons transition to a collective chaotic stripe phase, resulting in formation of multiple droplets along the interface with variable sizes [region IV in Fig. 3(d); see also Fig. 4(a) herein and Fig. S19 in Ref. [15]].

The results above, when combined, reveal that interfacial electrohydrodynamic effects generated by solitons in LCs can lead to jetting and droplet formation. Several factors distinguish our results from electrohydrodynamic instabilities at liquid-liquid interfaces reported in prior studies [26–28,33,39,40]. First, our observations support the hypothesis that solitonic emulsification arises from
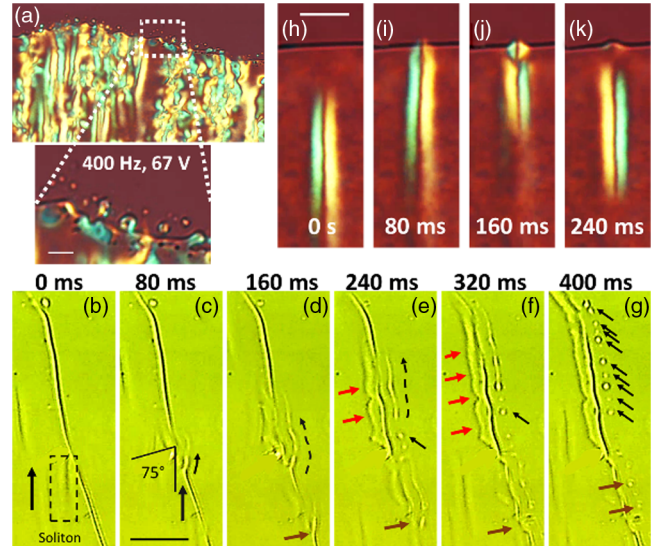
FIG. 4. (a) Formation of LC droplets in the presence of the chaotic striped phase. Inset in (a) shows the droplets. Scale bar 10 μm. (b)–(g) Bright-field images showing the nematic CCN-47–squalane interface following a collision with a soliton at glancing (75°) incidence. The dashed rectangle in (b) shows the incident soliton moving in a direction indicated by the black arrow. After the collision of the soliton with the LC interface, a long filament of LC is formed parallel to the interface, as shown in (c)–(e). In (e), the onset of breakup of the filament is evident (black arrow). The LC droplets are indicated by black arrows in (e)–(g). During growth of the LC jet, director perturbations [red arrows in (e) and (f)] propagate along the LC side of the interface. Brown arrows in (d)–(g) indicate the collision of a second soliton with the LC interface. Scale bar 30 μm. The optical contrast in the images was enhanced for ease of visualization. (h)–(k) Snapshots (cross polar) showing the reflection of a soliton that collides with the CCN-47–squalane interface at normal incidence. Scale bar 30 μm.

transduction of flexoelectric energy associated with localized strain of the LC director within a soliton into interfacial energy. While the interfacial response is consistent with a relaxation of charges that accumulate at the interface, the charges arise from flexoelectric polarization and not differences in ionic conductivity and dielectric permittivity (see S5 and Fig. S20 for experiments performed with added salts [15]). Second, in solitonic emulsification, the direction of LC jetting is determined by the direction of the propagating soliton, and not by the external electric field, which is applied tangential to the LC-isotropic oil interface. This contrasts to prior studies, where a nonzero component of the electric field normal to the interface, or a spatially nonuniform electric field, is needed to generate electrohydrodynamic instabilities [26,33]. The central role of the solitons in our experiments is further evidenced by the observation that the size of the soliton, rather than the magnitude of the applied field, determines the size of the generated LC drops. Finally, our observation that the LC jet bends toward the interface and is

accompanied by director perturbations on the LC side of the interface suggests the presence of a hydrodynamic coupling between the growing jet and LC director perturbation propagating along the LC interface (see below for additional discussion). Overall, our work serves as the first demonstration of the transduction of solitonic flexoelectric energy into the creation of fluid microstructures.

The observations reported above document one of several classes of interfacial phenomena that we observed to be triggered by collisions between LC solitons and deformable LC-isotropic interfaces. For example, when solitons impacted the LC-isotropic oil interface at grazing angles of incidence ($\theta > 70°$), we observed the formation of LC threads with lengths of 30 to 120 μm [Figs. 4(b)–4(g) herein and Fig. S21 [15]] and growth rates comparable to the velocities of the incident solitons (~300–400 μm/s). Additionally, inspection of Figs. 4(c)–4(e) reveals that, after a brief (80 ms) period of growth along the initial direction of soliton propagation, the threads bend to grow parallel to the LC-isotropic oil interface. The growth of the LC filament in the isotropic oil phase coincides with the propagation of the director fluctuation along the LC side of the interface [see highlighted regions in Figs. 4(d)–4(g)]. The threads were observed to routinely break into a series of small droplets [Figs. 4(b)–4(g) herein and Fig. S22 in Ref. [15]]. While the fragmentation of the jet into multiple droplets is consistent with a capillary instability [36,38,41], the formation of the LC thread is remarkable and provides additional evidence of a hydrodynamic coupling between the LC jet and director perturbation propagating along the LC interface. In other experiments, when solitons collided with the LC-oil interface at normal incidence, we observed the solitons to be reflected back into the LC phase without triggering the formation of a LC drop [Figs. 4(h)–4(k) herein and Fig. S23 [15]]. Overall, these observations highlight the rich range of phenomena that accompany the interactions of solitons with deformable fluid interfaces. These results also provide new ideas for the use of solitons in the design of active and adaptive soft matter by leveraging the dynamic response of interfaces in the presence of a focused source of energy.

---

*nla34@cornell.edu

[1] E. P. Solomon, C. E. Martin, D. W. Martin, and L. R. Berg, *Biology* (Cengage Learning, United States, 2018).

[2] B. Choy and D. D. Reible, *Diffusion Models of Environmental Transport* (CRC Press, United Kingdom, 2017).

[3] H. T. McMahon and J. L. Gallop, Membrane curvature and mechanisms of dynamic cell membrane remodelling, Nature (London) **438**, 590 (2005).

[4] Y. Shibata, J. Hu, M. M. Kozlov, and T. A. Rapoport, Mechanisms shaping the membranes of cellular organelles, Annu. Rev. Cell Dev. Biol. **25**, 329 (2009).

[5] T. Heimburg and A. D. Jackson, On soliton propagation in biomembranes and nerves, Proc. Natl. Acad. Sci. U.S.A. **102**, 9790 (2005).

[6] H. Kuwayama and S. Ishida, Biological soliton in multicellular movement, Sci. Rep. **3**, 1 (2013).

[7] L. V. Yakushevich, Is DNA a nonlinear dynamical system where solitary conformational waves are possible?, J. Biosci. **26**, 305 (2001).

[8] B. X. Li, V. Borshch, R. L. Xiao, S. Paladugu, T. Turiv, S. V. Shiyanovskii, and O. D. Lavrentovich, Electrically driven three-dimensional solitary waves as director bullets in nematic liquid crystals, Nat. Commun. **9**, 2912 (2018).

[9] B. X. Li, R. L. Xiao, S. Paladugu, S. V. Shiyanovskii, and O. D. Lavrentovich, Three-dimensional solitary waves with electrically tunable direction of propagation in nematics, Nat. Commun. **10**, 3749 (2019).

[10] L. Lam and J. Prost, *Solitons in Liquid Crystals* (Springer Science & Business Media, New York, 1992).

[11] K. B. Migler and R. B. Meyer, Solitons and Pattern Formation in Liquid Crystals in a Rotating Magnetic Field, Phys. Rev. Lett. **66**, 1485 (1991).

[12] C. Zheng and R. B. Meyer, Structure and dynamics of solitons in a nematic liquid crystal in a rotating magnetic field, Phys. Rev. E **56**, 5553 (1997).

[13] S. Das, S. Roh, N. Atzin, A. Mozaffari, X. Tang, J. J. De Pablo, and N. L. Abbott, Programming solitons in liquid crystals using surface chemistry, Langmuir **38**, 3575 (2022).

[14] Y. Shen and I. Dierking, Dynamics of electrically driven solitons in nematic and cholesteric liquid crystals, Commun. Phys. **3**, 14 (2020).

[15] See Supplemental Material at http://link.aps.org/supplemental/10.1103/PhysRevLett.131.098101 for a discussion on the mechanisms of soliton formation and for the effect of added salts on the formation of LC jets and emulsion drops, which includes Refs. [16–19].

[16] A. L. Alexe-Ionescu, Flexoelectric polarization and second order elasticity for nematic liquid crystals, Phys. Lett. A **180**, 456 (1993).

[17] B. X. Li, R. L. Xiao, S. V. Shiyanovskii, and O. D. Lavrentovich, Soliton-induced liquid crystal enabled electrophoresis, Phys. Rev. Res. **2**, 013178 (2020).

[18] F. Yalcinkaya, B. Yalcinkaya, and O. Jirsak, Influence of salts on electrospinning of aqueous and nonaqueous polymer solutions, J. Nanomater. **2015** (2015).

[19] P. K. Bhattacharjee and G. C. Rutledge, Electrospinning and polymer nanofibers: Process fundamentals, in *Comprehensive Biomaterials* (Elsevier, New York, 2011), pp. 497–512.

[20] Y. Shen and I. Dierking, Dynamic dissipative solitons in nematics with positive anisotropies, Soft Matter **16**, 5325 (2020).

[21] H. R. Brand, C. Fradin, P. L. Finn, W. Pesch, and P. E. Cladis, Electroconvection in nematic liquid crystals:

Comparison between experimental results and the hydrodynamic model, Phys. Lett. A **235,** 508 (1997).

[22] Y. Shen and I. Dierking, Recent progresses on experimental investigations of topological and dissipative solitons in liquid crystals, Crystals **12,** 94 (2022).

[23] Y. Shen and I. Dierking, Electrically tunable collective motion of dissipative solitons in chiral nematic films, Nat. Commun. **13,** 1 (2022).

[24] N. Atzin, A. Mozaffari, X. Tang, S. Das, N. L. Abbott, and J. J. de Pablo, A minimal model of solitons in nematic liquid crystals, arXiv:2210.08666v1.

[25] X. Tang, A. Mozaffari, N. Atzin, S. Das, N. L. Abbott, and J. J. de Pablo, Generation and propagation of solitary waves in nematic liquid crystals, arXiv:2211.01453v1.

[26] A. Bandopadhyay and U. Ghosh, Electrohydrodynamic phenomena, J. Indian Inst. Sci. **98,** 201 (2018).

[27] J. U. Park *et al.*, High-resolution electrohydrodynamic jet printing, Nat. Mater. **6,** 782 (2007).

[28] Q. Brosseau and P. M. Vlahovska, Streaming from the Equator of a Drop in an External Electric Field, Phys. Rev. Lett. **119,** 034501 (2017).

[29] A. R. Thiam, N. Bremond, and J. Bibette, Breaking of an Emulsion under an ac Electric Field, Phys. Rev. Lett. **102,** 188304 (2009).

[30] M. S. Abbasi, R. Song, S. M. Kim, H. Kim, and J. Lee, Mono-emulsion droplet stretching under direct current electric field, Soft Matter **15,** 2328 (2019).

[31] G. Chen, P. Tan, S. Chen, J. Huang, W. Wen, and L. Xu, Coalescence of Pickering Emulsion Droplets Induced by an Electric Field, Phys. Rev. Lett. **110,** 064502 (2013).

[32] P. Soni, V. A. Juvekar, and V. M. Naik, Investigation on dynamics of double emulsion droplet in a uniform electric field, J. Electrost. **71,** 471 (2013).

[33] M. S. Abbasi, R. Song, S. Cho, and J. Lee, Electrohydrodynamics of emulsion droplets: Physical insights to applications, Micromachines **11,** 1 (2020).

[34] G. F. Scheele and B. J. Meister, Drop formation at low velocities in liquid-liquid systems: Part I. Prediction of drop volume, AIChE J. **14,** 9 (1968).

[35] A. H. P. Skelland and P. G. Walker, The effects of surface active agents on jet breakup in liquid-liquid systems, Can. J. Chem. Eng. **67,** 762 (1989).

[36] A. S. Utada, A. Fernandez-Nieves, H. A. Stone, and D. A. Weitz, Dripping to Jetting Transitions in Coflowing Liquid Streams, Phys. Rev. Lett. **99,** 094502 (2007).

[37] L. Cai, J. Marthelot, and P. T. Brun, An unbounded approach to microfluidics using the Rayleigh–Plateau instability of viscous threads directly drawn in a bath, Proc. Natl. Acad. Sci. U.S.A. **116,** 22966 (2019).

[38] J. K. Nunes, S. S. H. Tsai, J. Wan, and H. A. Stone, Dripping and jetting in microfluidic multiphase flows applied to particle and fibre synthesis, J. Phys. D **46,** 114002 (2013).

[39] R. T. Collins, J. J. Jones, M. T. Harris, and O. A. Basaran, Electrohydrodynamic tip streaming and emission of charged drops from liquid cones, Nat. Phys. **4,** 149 (2007).

[40] M. Z. Bazant, Electrokinetics meets electrohydrodynamics, J. Fluid Mech. **782,** 1 (2015).

[41] J. R. Lister and H. A. Stone, Capillary breakup of a viscous thread surrounded by another viscous fluid, Phys. Fluids **10,** 2758 (1998).